

Constraints on the dark energy equation of state from the separation of CMB peaks and the evolution of α .

Seokcheon Lee

*School of Physics and Astronomy,
University of Minnesota, Minneapolis, MN 55455, USA*

Abstract

We introduce a simple parametrization of the dark energy equation of state, ω , which is motivated from theory and recent experimental data. The theory is related to the tracker solution to alleviate the fine tuning problem. Recent experimental data indicates that the present value of ω is close to -1 . We analyze the evolution of ω from the separation of CMB peaks and the time variation of the fine structure constant, α . We find that $-1.00 \leq \omega^{(0)} \leq -0.971_{-0.027}^{+0.017}$ and $1.76_{-0.42}^{+0.29} \times 10^{-4} \leq (d\omega/dz)_{z=0} \leq 0.041_{-0.037}^{+0.016}$ at 95% confidence level (CL).

1 Introduction

Recent cosmological observations show that a component with negative pressure (dark energy) should be added to the matter component to give the critical density today [1]. The cosmological constant and/or a quintessence field are the most commonly accepted candidates for dark energy. The latter is a dynamical scalar field leading to a time dependent equation of state, ω .

There are certain hopes that quintessencelike models may help alleviate the severe fine-tuning problem associated with the cosmological constant and that the nature of dark energy can be understood by measuring the behavior of ω with respect to time [2, 3]. But it may not be practical to test every single quintessence model by using experimental data. So a model independent approach for quintessence could be an effective way to study the properties of dark energy.

To investigate the cosmological evolution of ω , we may use the relation between the luminosity distance and redshift (z), which can be obtained from type Ia supernovae (SNe Ia) as standard candles [4]. In this case, the distribution of the supernovae (SNe) along z provides a clue for the determination of ω . The dependency of the luminosity distance on ω increases in proportion to z . The separation of cosmic microwave background (CMB) peaks can also be used to investigate ω because the location of peaks depends on the amount of dark energy today and at last scattering as well as ω [5]. In addition, the cosmological evolution of the fine structure constant, α may be used to determine the z dependence of ω [6]. The advantage of using α is that there will not be any degeneracies between parameters due to the multiple integrals as in the determination of luminosity distance [7].

A number of parametrizations of ω have been used to probe the nature of dark energy. The simplest is the averaged value $\bar{\omega}$, defined as $\bar{\omega} = \int \omega(z)\Omega_\phi(z)dz / \int \Omega_\phi(z)dz$ where Ω_ϕ is dark energy density contrast. This parametrization is weighted by Ω_ϕ indicating that ω is more significant if ρ_ϕ is a larger part of the critical density. If ω does not change during the recent history of the universe, when Ω_ϕ is comparable to matter density (Ω_m), then the average $\bar{\omega}^{(0)}$ will be equal to present value, $\omega^{(0)}$. The next intuitive method is a first order Taylor expansion of ω in z , $\omega(z) = \omega|_{z=0} + d\omega/dz|_{z=0}z$. This diverges at large value of z , which makes it only useful for low z analyses, such as SNe [8]. Another simple parametrization is $\omega = \omega_0 + \omega_1 z / (1 + z)^p$ where $p = 1, 2$. When p is equal to one, $\omega_0 + \omega_1$ is constrained as a negative value to satisfy SNe data. In addition, Ω_ϕ at decoupling should be negligible based on WMAP [9]. However with this constraint we can not get a small value of Ω_ϕ at decoupling. The $p = 2$ case can solve this problem [10]. A simple extension of the previous cases is given by $\omega(a) = \omega_0\omega_1(a^q + a_s^q) / (\omega_1 a^q + \omega_0 a_s^q)$, which includes huge flexibility and the intuitive role of each parameter [8]. In this case, both ω_0 and ω_1 should have the same (negative) signs. Otherwise, ω will diverge at $a^q = -(\omega_0/\omega_1)a_s^q$. There have

also been more complicated parametrizations [11].

We introduce a new parametrization of ω , which looks similar to that in [8]. However it is necessary that the sign of ω_0 is opposite to that of ω_1 to have a smoothly changing ω . We will not consider the case of $\omega < -1$, which can be obtained in scalar-tensor gravity models [12], phantom models [13], and brane models [14].

This paper is organized as follows. In the next section we introduce a parametrization of ω and specify some of its parameters. By changing these parameters we can mimic several quintessence models. In section 3, we use CMB peaks to restrict the parameters. We check the time variation of α based on this parametrization in section 4. Our conclusion is in the last section.

2 Parametrization of ω

For cosmological evolution equations, it is convenient to introduce a variable x as the logarithm of the scale factor a ,

$$x = \ln a = -\ln(1+z) \tag{2.1}$$

where we choose the present scale factor $a^{(0)} = 1$. We propose a simple parametrization of the dark energy equation of state,

$$\omega(a) = \omega_r \frac{\omega_0 a^q + a_c^q}{a^q + a_c^q} \implies \omega(x) = \omega_r \frac{\omega_0 \exp(qx) + \exp(qx_c)}{\exp(qx) + \exp(qx_c)} \tag{2.2}$$

where ω_r , ω_0 , a_c (equally x_c), and q are constants. Instead of leaving ω_r and ω_0 as arbitrary constants, we adopt the tracking condition in the early universe *i.e.* ω changes as that of radiation ($\omega = \omega_r = 1/3$). Also we use the experimental evidence which indicates ω approaches negative one at present. These constraints fix two constants in Eq. (2.2) :

$$\omega_r = \frac{1}{3}, \quad \omega_0 = -3 \tag{2.3}$$

There remain two arbitrary constants a_c and q , which describe the scale factor at changeover and the duration of it respectively. When a is close to a_c , ω starts to decrease and ω reaches to -1 as a approaches $a^0 = 1$. We call a transition of ω from the tracking region to the $\omega \sim -1$ region as changeover. We can also narrow the range of the a_c value, when we consider the fact that initial value of ρ_ϕ is expected to be 120 orders of magnitude larger than the present value. We will see this in the next section. As we can see in Eq. (2.2), for larger value of q , the duration of changeover of ω decreases. During early times $\omega \simeq \omega_r$ and it stays with same value before a approaches a_c . ω will approach $\omega_r \times \omega_0$ when $a \gg a_c$. This is the reason we choose the values in (2.3). If a_c is too close to

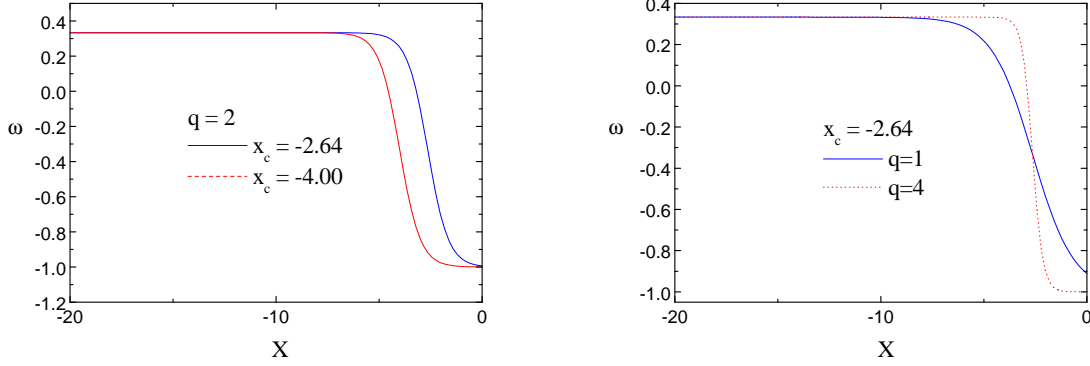


Figure 1: The evolution of ω . (a) The dependence on the changeover scale, x_c of the evolution of ω . A smaller value of x_c means an earlier change of ω shown as the dashed line. (b) The dependence on q of the evolution of ω . The solid line ($q = 1$) shows a slower change than the dashed one ($q = 4$). That means the duration of the changeover becomes longer as the value of q becomes smaller.

$a^{(0)} = 1$, then the present value of ω will not be close to -1 for small q . Thus there is a limit to x_c for each value of q . The cosmological evolution of ω due to this parametrization for different values of q and x_c are shown in Fig. 1 and Fig. 2. The effect of x_c on the evolution of ω is shown in Fig. 1 (a). A smaller value of x_c gives an earlier change of ω . As x_c decreases, the period of $\omega = -1$ increases. A smaller value of q shows a slower change of ω as in Fig. 1(b). For a specific value of $x_c = -2.64$, we require $q \geq 0.62$ to satisfy WMAP data. For larger values of q we can still get $\omega^{(0)} = -1$ even with large x_c (*i.e.* the duration of changeover is small). From Fig. 2 we show the minimum value of q (q_{\min}) for each x_c to satisfy WMAP data ($\omega^{(0)} < -0.78$). For a smaller value of x_c we allow a smaller value of q_{\min} to satisfy WMAP due to the fact that ω changes early and it takes more time for ω to reach today when x_c is small. This is shown in Fig. 2(a). We also show the restriction of q for a specific value of x_c in Fig. 2(b). The advantages of this parametrization are its simplicity and the possibility of mimicking various models. However this parametrization cannot account for an oscillating ω , which can be obtained from a $\cosh(\phi)$ -potential and the coupled cases with general potentials [15, 16]. Thus this parametrization is good only for monotonically varying ω .

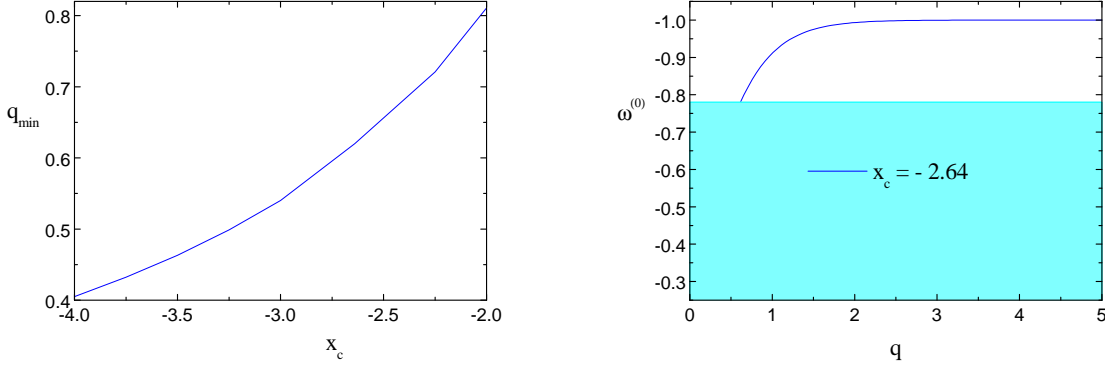


Figure 2: The present value of the equation of state, $\omega^{(0)}$. (a) q_{\min} means the minimum value of q for each different value of x_c to satisfy WMAP data ($\omega^{(0)} < -0.78$) [9]. (b) The shaded region is forbidden from WMAP. From this we can make the restriction $q \geq 0.62$ when $x_c = -2.64$. The reason for the choice of this specific value of x_c will be shown later.

3 CMB peak spacing

The location of the acoustic peaks and the spacing between the peaks can be estimated if an adiabatic initial condition and a flat universe are assumed [5, 17]. The acoustic scale, l_A is given by the simple formula

$$l_A \equiv \pi \frac{d_A}{s} = \pi \frac{\tau_0 - \tau_{ls}}{s} = \pi \frac{\tau_0 - \tau_{ls}}{\bar{c}_s \tau_{ls}} \quad (3.1)$$

where d_A is the angular size distance to decoupling, τ_0 and τ_{ls} are the conformal time today and at last scattering. The sound horizon at decoupling is given by $s = \bar{c}_s \tau_{ls}$ and the average sound speed before last scattering is,

$$\bar{c}_s = \frac{\int_0^{\tau_{ls}} c_s d\tau}{\tau_{ls}} \quad \text{where} \quad c_s^{-2} = 3 + \frac{9 \rho_b(t)}{4 \rho_r(t)} \quad (3.2)$$

where ρ_b and ρ_r are the baryon and photon energy densities, respectively. The location of the m -th peak and trough is slightly shifted by driving effects and this can be written as [18] ;

$$l_m \equiv l_A(m - \varphi_m) \equiv l_A(m - \bar{\varphi} - \delta\varphi_m) \quad (3.3)$$

where $\bar{\varphi} \equiv \varphi_1$ is the overall peak shift and $\delta\varphi_m$ is the shift of the m -th peak relative to the first. We attach the fitting formulae in the appendix for the sake of completeness. To see the effect of quintessence, we start from the Friedmann equation.

$$H^2 = \frac{1}{3\bar{M}^2}(\rho_\phi + \rho_r + \rho_m) \equiv \frac{1}{3\bar{M}^2}\rho_{cr} \quad (3.4)$$

where H is the Hubble expansion rate, $\bar{M}^2 = M_p^2/8\pi$ is a reduced Planck mass, and ρ_i are the energy densities of each component. From the continuity equation of energy density we

find,

$$d \ln \rho_\phi = -3(1 + \omega)dx. \quad (3.5)$$

This equation can be integrated using the parametrization of ω in Eq. (2.2) :

$$\rho_\phi(x) = \rho_\phi^{(0)} \exp(-4x) \left(\frac{\exp(qx) + \exp(qx_c)}{1 + \exp(qx_c)} \right)^{4/q} = \rho_\phi^{(0)} a^{-4} \left(\frac{a^q + a_c^q}{1 + a_c^q} \right)^{4/q} \quad (3.6)$$

where $\rho_\phi^{(0)}$ is the dark energy density today. We also find the dark energy density contrast (Ω_ϕ) from the above equation (3.6).

$$\Omega_\phi(a) = \frac{\rho_\phi}{\rho_{cr}} = \left[1 + \frac{\Omega_m^{(0)}}{\Omega_\phi^{(0)}} (a + a_{eq}) \left(\frac{a^q + a_c^q}{1 + a_c^q} \right)^{-4/q} \right]^{-1} \quad (3.7)$$

where $\Omega_i^{(0)} = \rho_i^{(0)}/\rho_{cr}^{(0)}$ is the present energy density contrast of each component. In the second equality we use the relation $\Omega_r^{(0)} = \Omega_m^{(0)} a_{eq}$ where a_{eq} is the scale factor when the radiation and matter densities are equal.

Table 1: Cosmological parameters used in the analysis. We use WMAP data [9].

$\Omega_\phi^{(0)}$	$\Omega_m^{(0)}$	$\Omega_b^{(0)} h^2$	z_{ls}	z_{eq}	n_s
0.73	0.27	0.0224	1089	3233	0.93

From Eq. (3.6), we can see that the dark energy density, ρ_ϕ evolves as the energy density of radiation ($\rho_r \propto a^{-4}$) during $a \ll a_c$. ρ_ϕ starts to departure from this behavior as a approaches a_c . This explains the tracking behavior of dark energy during the radiation dominated era. The cosmological evolution of the dark energy density is shown in Fig. 3. ρ_ϕ is changed by 120 orders of magnitude through the entire history of the universe. Also from Eq. (3.6) we know that the initial value of dark energy, $\rho_\phi^{(0)} (a_c/a_i)^4$ is independent of q , where a_i is the scale factor at the beginning of the universe. If we use the fact that $\rho_\phi^i/\rho_\phi^{(0)} \sim 10^{120}$ and $a_i \sim 10^{-32}$, then we find that a_c should be approximately 10^{-2} (equally $x_c \sim -4$). We can make further restriction on a_c from the following consideration. To be compatible with observational data, the energy density of quintessence must be subdominant during Big Bang Nucleosynthesis (BBN) [3], $\Omega_\phi^{(BBN)}(x \sim -23) \leq 0.2$ at $T \sim 1$ MeV. If we consider the fact that $1 \gg a_c \gg a_{eq} \gg a_{BBN}$, then the equation of dark energy density contrast (3.7) is approximately :

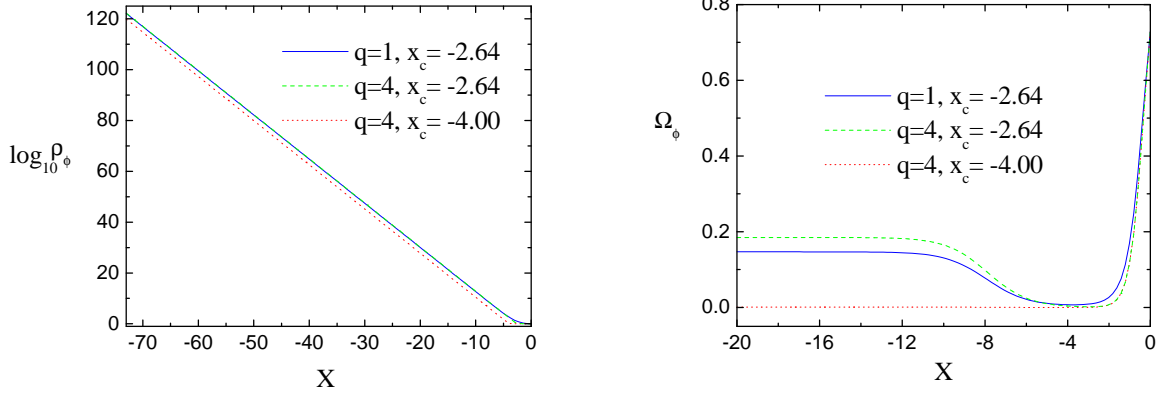


Figure 3: (a) The cosmological evolution of ρ_ϕ for specific q and x_c values. For other values of these parameters, we can get similar behaviors which can account for 120 orders of magnitude change in ρ_ϕ . (b) The evolution of Ω_ϕ when we fix $\Omega_\phi^{(0)} = 0.73$. When $x_c = -2.64$, a smaller value of $q = 1$ (solid line) shows a slower change in Ω_ϕ at late universe compared to $q = 4$ (dashed line). For a smaller value of $x_c = -4.00$ (dotted line), Ω_ϕ is negligible during early universe for any value of q .

$$\Omega_\phi(a_{BBN}) \simeq \left[1 + \frac{\Omega_m^{(0)} a_{eq}}{\Omega_\phi^{(0)} a_c^4} \right]^{-1} \leq 0.2 \implies a_c \simeq \left(\frac{1 - \Omega_\phi^{(0)}}{\Omega_\phi^{(0)}} \frac{\Omega_\phi^{(BBN)}}{1 - \Omega_\phi^{(BBN)}} a_{eq} \right)^{1/4} \leq 0.073 \quad (3.8)$$

This corresponds to $x_c \leq -2.60$ independent of q . As previously mentioned, the slope of ρ_ϕ during the radiation dominated era has nothing to do with a_c or q . The effect of q appears when a approaches a_c . This effect on ρ_ϕ is hardly seen as in Fig. 3(a) due to degeneracy. However we can see this effect from Fig. 3(b). A larger value of q (dashed line) gives the steeper change in ρ_ϕ and Ω_ϕ than those of a smaller value of q (solid line) at late time. As we can see in the equation (3.8), the Ω_ϕ value depends only on a_c before a reaches to a_{eq} . Thus for the smaller value of a_c , Ω_ϕ value will be more close to the value of cosmological constant, Ω_Λ . The evolution of dark energy density shows degeneracy between the different choice of parameters on ω . This may require additional experimental data to investigate the evolution of ω instead of using SNe. Because SNe data is analyzed by the luminosity distance, which mainly depends on ρ_ϕ . In the above graphs we fix $\Omega_\phi^{(0)} = 0.73$. Now we rewrite the equation (3.4) by using conformal time, τ :

$$\begin{aligned} \left(\frac{da}{d\tau} \right)^2 &= H_0^2 \left\{ \Omega_r^{(0)} + \Omega_m^{(0)} a + \Omega_\phi^{(0)} \left(\frac{a^q + a_c^q}{1 + a_c^q} \right)^{4/q} \right\} = H_0^2 \left\{ \Omega_m^{(0)} (a + a_{eq}) + \Omega_\phi^{(0)} \left(\frac{a^q + a_c^q}{1 + a_c^q} \right)^{4/q} \right\} \\ &= H_0^2 \left\{ (1 - \Omega_r^{(0)} - \Omega_\phi^{(0)}) (a + a_{eq}) + \Omega_\phi^{(0)} \left(\frac{a^q + a_c^q}{1 + a_c^q} \right)^{4/q} \right\} \end{aligned} \quad (3.9)$$

where H_0 is the present value of Hubble parameter. If we use WMAP data $\Omega_r^{(0)} \simeq 4.9 \times 10^{-5}$, $\Omega_m^{(0)} \simeq 0.27$, $\Omega_\phi^{(0)} \simeq 0.73$, and $a_{eq} = 1/(1 + z_{eq}) = 1/3234$, then we have the following

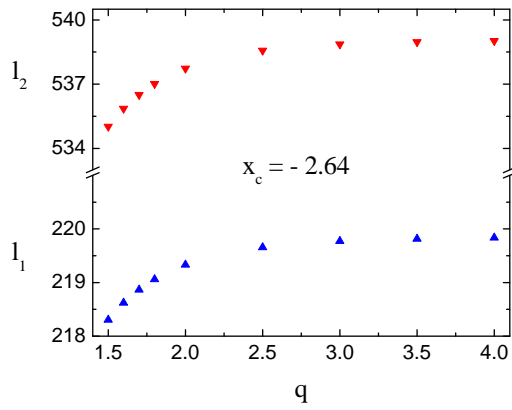


Figure 4: The locations of the first and the second CMB peaks. The uptriangles indicate the first peaks, l_1 and the downtriangles show the second peaks, l_2 as a function of q . Both l_1 and l_2 converge as q increases.

approximation of the above equation (3.9).

$$\left(\frac{da}{d\tau}\right)^2 \simeq H_0^2 \left\{ (1 - \Omega_\phi^{(0)})(a + a_{eq}) + \Omega_\phi^{(0)} \left(\frac{a^q + a_c^q}{1 + a_c^q}\right)^{4/q} \right\} \neq H_0^2 \left\{ (1 - \Omega_\phi^{(0)})a + \Omega_\phi^{(0)} \left(\frac{a^q + a_c^q}{1 + a_c^q}\right)^{4/q} \right\} \quad (3.10)$$

The approximation comes from the fact that $\Omega_r^{(0)} \ll \Omega_{m,\phi}^{(0)}$. We indicate the inequality between the first and the second expressions, which is frequently used in the literature. The numerical difference between two expressions is not negligible for the specific values of a_c and q . So we will use the first (accurate) expression in the following calculations. From this equation we can find the numerical value of τ when a_c and q are fixed.

$$d\tau = H_0^{-1} \left((1 - \Omega_\phi^{(0)})(a + a_{eq}) + \Omega_\phi^{(0)} \left(\frac{a^q + a_c^q}{1 + a_c^q}\right)^{4/q} \right)^{-1/2} da \quad (3.11)$$

Table 2: The spacing and the location of the CMB peaks for several values of q when $x_c = -2.64$. Here we use the cosmological parameters in Table 1.

x_c	q	l_A	l_1	l_2	$\Omega_\phi^{l_s}(10^{-2})$
-2.64	1.5	300.8	218.3	535.0	5.17
	2	302.4	219.3	537.7	5.36
	3	303.1	219.8	538.9	5.40
	4	303.1	219.8	539.0	5.41

By using the above equations we can find the acoustic scale (l_A), the locations of the first two peaks (l_1, l_2), and Ω_ϕ at last scattering ($\Omega_\phi^{l_s}$). They are given in Table 2 and Fig.

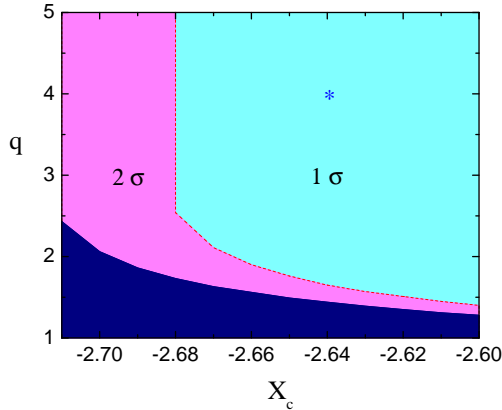


Figure 5: The 68 % (light shaded) and 95 % (medium shaded) confidence allowed regions for x_c and q using WMAP data. Asterisk indicates the best fit values ($x_c = -2.64$, $q = 4.01$). The dark shaded regions are out of 2σ confidence level. The constraint from the dark energy density at BBN determines the upper limit on x_c (≤ -2.60). The lower limit of x_c (> -2.72) is obtained from χ^2 -analysis. There is no upper limit on q values from WMAP. However we can obtain the upper limit on q from the analysis of the time varying α in the following section.

4. For a value of x_c , the location of CMB peaks depends on q -values. However CMB peak values converge to some values as q increases. From WMAP measurements the acoustic scale and the locations of the first two peaks are [9] :

$$l_A = 301 \pm 1, \quad l_1 = 220.1 \pm 0.8, \quad l_2 = 546 \pm 10. \quad (3.12)$$

If we assume that the errors are Gaussian and uncorrelated, then we can find a χ^2 -statistic

$$\chi^2 = \sum_i \frac{(l_{i,obs} - l_{i,theory})^2}{\sigma_i^2} \quad (3.13)$$

where $l_{i,obs}$ is the observational data of each peak, $l_{i,theory}$ is the theoretical value of l_i , and σ_i is the statistical uncertainty for each peak. The likelihoods for the parameters (q, x_c) of the parametrization given in (2.2) are calculated from χ^2 so that the 68 % and 95 % confidence regions are determined by $\Delta\chi^2 \equiv \chi^2 - \chi_0^2 = 2.30$ and 6.17 respectively. χ_0^2 is χ^2 for the best fit model found. The best fit values to the WMAP data is obtained from $x_c = -2.64$ and $q = 4.01$. The likelihood contours for WMAP are shown in Fig. 5. The 68 % (light shaded) and 95 % (medium shaded) confidence allowed regions for x_c and q are shown using WMAP data. There is no upper limit on q values for several x_c values. From this we find at 95 % CL :

$$\omega^{(0)} \leq -0.971_{-0.027}^{+0.017}, \quad \left(\frac{d\omega}{dz} \right)_{z=0} \leq 0.041_{-0.037}^{+0.016} \quad (3.14)$$

ω is almost a constant at present, which is consistent with recent observation [19].

4 Time variation of the fine structure constant

In this section we consider the ϕ -dependence of the gauge couplings in Standard Model (SM), $B_F(\phi)$ [16]. The interaction of a light scalar field ϕ with electromagnetic field is represented in the Lagrangian as $\mathcal{L}_{EM} = -B_F(\phi)F_{\mu\nu}F^{\mu\nu}/4$, where $F^{\mu\nu}$ is the electromagnetic field-strength tensor. The main assumption in this work is that all functions $B_F(\phi)$ and $V(\phi)$ admit a common extremum, which is a generalization of Damour-Nordtvedt and Damour-Polyakov constructions [20]. To this end, we proposed an ansatz that would relate $B_F(\phi)$ and $V(\phi)$.

$$B_F(\phi) = \left(\frac{b_F + V(\phi)/V_0}{1 + b_F} \right)^{n_F}, \quad \text{where } b_F + 1 > 0 \quad (4.1)$$

where n_F and b_F are two dimensionless parameters allowing us to cover a wide range of possibilities. We will assume that dark energy is a quintessence field and its potential is parameterized by ω . So instead of introducing a potential of the scalar field, we will use ω . We can rewrite (4.1) by using the parametrization of ω (2.2). We also use the relation between the potential $V(\phi)$ and the energy density ρ_ϕ of the scalar field,

$$V(\phi) = \frac{(1-\omega)}{2}\rho_\phi \Rightarrow V(x) = \rho_\phi^{(0)} \exp(-4x)A_1(x)A_2(x) \quad (4.2)$$

where

$$A_1(x) = \left(\frac{\exp(qx) + \exp(qx_c)}{1 + \exp(qx_c)} \right)^{4/q}, \quad (4.3)$$

$$A_2(x) = \frac{3 \exp(qx) + \exp(qx_c)}{3(\exp(qx) + \exp(qx_c))} \quad (4.4)$$

With these equations (2.2), (3.6), and (4.2), we can rewrite the gauge coupling in Eq (4.1) as follow,

$$B_F(x) = \left(\frac{b_F + \exp(-4x)A_1(x)A_2(x)/A_2(0)}{1 + b_F} \right)^{n_F} \quad (4.5)$$

where we assume that $V_0 = V(x=0)$ to satisfy $B_F(0) = 1$. We can find the time variation of the fine structure constant by using the following relation between B_F and α ,

$$\frac{\Delta\alpha}{\alpha} \equiv \frac{\alpha(x) - \alpha(0)}{\alpha(0)} = \frac{1}{B_F(x)} - 1. \quad (4.6)$$

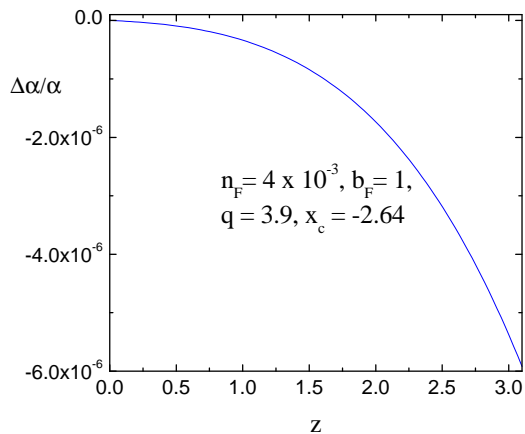


Figure 6: A typical evolution $\Delta\alpha/\alpha$ for specific n_F , b_F , q and x_c values. We can get similar behaviors with other values of parameters. n_F and b_F values are obtained from the result of Murphy *et al.* Several values of $\Delta\alpha/\alpha$ for various choices of the parameters at different z are indicated in Table 3.

From equations (4.5) and (4.6), we find

$$\frac{\Delta\alpha}{\alpha} = \left(\frac{1 + b_F}{b_F + \exp(-4x)A_1(x)A_2(x)/A_2(0)} \right)^{n_F} - 1 \quad (4.7)$$

Table 3: The values of $\Delta\alpha/\alpha$ at the different z for the several values of q when $x_c = -2.64$. Here we use the QSOs result to fix other values [21]. n_F has been scaled by a factor of 10^3 , $\Delta\alpha/\alpha$ values have been scaled by a factor of 10^6 except the value at decoupling $(\Delta\alpha/\alpha)_{ls}$, which is given in the last column without any scaling.

x_c	q	n_F	b_F	$(\frac{\Delta\alpha}{\alpha})_3$	$(\frac{\Delta\alpha}{\alpha})_{1.5}$	$(\frac{\Delta\alpha}{\alpha})_{0.45}$	$(\frac{\Delta\alpha}{\alpha})_{0.14}$	$(\frac{\Delta\alpha}{\alpha})_{1089}$
-2.64	3	4.25	11	-5.4	-1.25	-0.017	-0.041	-0.057
		0.71	1	-5.4	-1.26	-0.017	-0.042	-0.011
	3.5	3.68	3	-5.4	-1.01	-0.023	-0.025	-0.053
		1.84	1	-5.4	-1.01	-0.023	-0.025	-0.028
	3.9	4.01	1	-5.4	-0.84	-0.016	-0.016	-0.060

In Table 3, we display $\Delta\alpha/\alpha$ values at different redshifts for the various parameters. Especially we show specific results for $x_c = -2.64$, because this gives the best-fit value for the separation of CMB peaks as explained in the previous section. $\Delta\alpha/\alpha$ at the cosmic microwave background epoch, which is constrained as $(\Delta\alpha/\alpha)_{ls} \geq -0.06$ [22] are shown in the last column. There are four parameters (n_F , b_F , x_c , and q) to be fixed. In Fig. 6 we

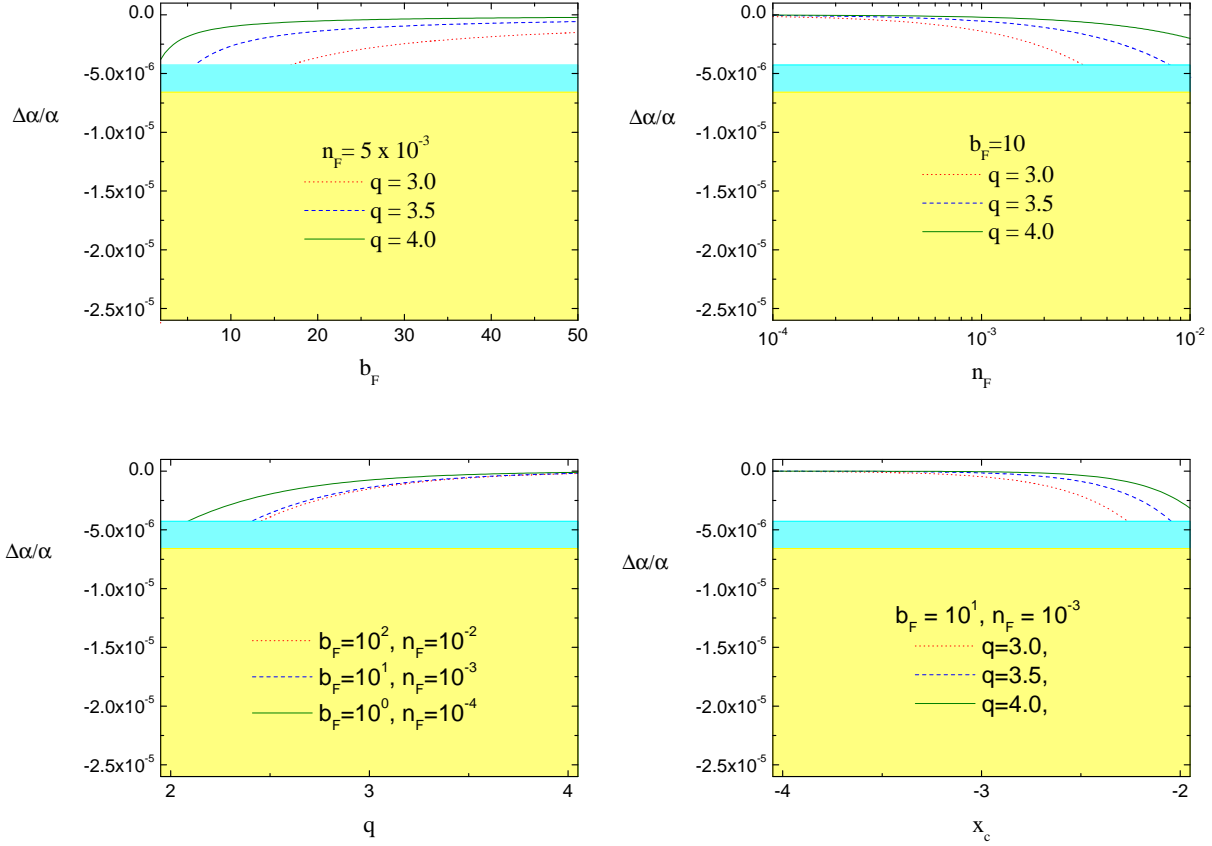


Figure 7: The cosmological evolution of α for the various parameters. Murphy *et al* data (medium shaded) is used in all of the figures, $(\Delta\alpha/\alpha)_{z=3} = (-0.543 \pm 0.116) \times 10^{-6}$. We use $x_c = -2.64$ for all of the graphs except (d). (a) The evolution of $\Delta\alpha/\alpha$ with respect to $b_F \geq 1$ for $n_F = 5 \times 10^{-3}$. When $q = 3$ (dotted line) α changes slower than when $q = 4$ (solid line). Thus we have more acceptable values of b for the smaller q ($10.6 \leq b_F \leq 16.9$ when $q = 3$). (b) The effect of changing n_F on $\Delta\alpha/\alpha$ while we fix $b_F = 10$. (c) and (d) the effect of varying q and x_c on the variation of α , respectively.

show a typical evolution of $\Delta\alpha/\alpha$ for a specific set of four parameters (*i.e.* $n_F = 4 \times 10^{-3}$, $b_F = 1$, $q = 3.9$, and $x_c = -2.64$). We can change four parameters to explain the effect on the evolution of α . However it is impossible to fix all four parameters at once. Thus we show the effect of the changing each parameter with fixing all other parameters at each time. We see that smaller values of q lead to more room for the parameter space regions of n_F and b_F , because smaller values of q lead to slower change in α . For given q -values, there may not be any solution to fit experimental data as shown in the first panel of Fig. 7. However as we increase the b_F -values we can satisfy the experimental data. We have larger b_F range for smaller values of q . Similar consideration can be made for varying n_F . For example, even though the dotted lines ($q = 3$) in the second panel does not fit experimental data when $n_F \geq 3 \times 10^{-3}$, as we decrease n_F we can recover the suitable $\Delta\alpha/\alpha$ for given q and x_c . The medium shaded regions of each panel are allowed from Murphy *et al*, $(\Delta\alpha/\alpha)_{z=3} = (-0.543 \pm 0.116) \times 10^{-5}$ [21]. The effect of changing q and x_c are shown in (c) and (d) of Fig. 7. As we expect there is lots of room for the choice of q and x_c because we have extra degrees of freedom (n_F and b_F) to be fixed in addition to the original parameters of ω . However combined with the analysis of the separation of CMB peaks, the parameters on gauge coupling are much narrowed as in Table 3. We can make the allowed regions for n_F and b_F from the narrowed parameter spaces of a_c and q . This is indicated in Fig. 8. The sloped lines are obtained from the normalization of Murphy *et al* data for the given q values when x_c is fixed as -2.64 . The vertical lines for each q come from both the CMB bound on α and the assumption of $b \geq 1$. There is only one allowed value $b_F = 1$ for $q = 3.9$ (solid line). This gives the upper limit on $q \leq -3.9$, which we can use for the consideration of CMB peaks. For $q = 3$ (dotted line), there are more parameter spaces to satisfy the constraints. In this case b_F can be increased up to 11. Obviously this gives much narrower parameter spaces for each parameter compared to Fig. 7. Now we can restrict $(n_F, b_F) \sim (10^{-3}, 1)$ as in [16] and $1.5 \leq q \leq 3.9$ for $x_c = -2.64$.

5 Conclusions

We have introduced a simple parametrization of ω based on both theory and experiment. A tracking solution is proposed to alleviate the fine tuning problem and the present value of ω is observed to be close to -1 . We have analyzed the separation of CMB peaks and the time variation of the fine structure constant with this parametrization. We have obtained the constraints of the parameters of ω from these analyses which use both low-redshifts and high-redshifts data. We have been able to use the analytically integrated value of the dark energy density contrast, Ω_ϕ from this parametrization.

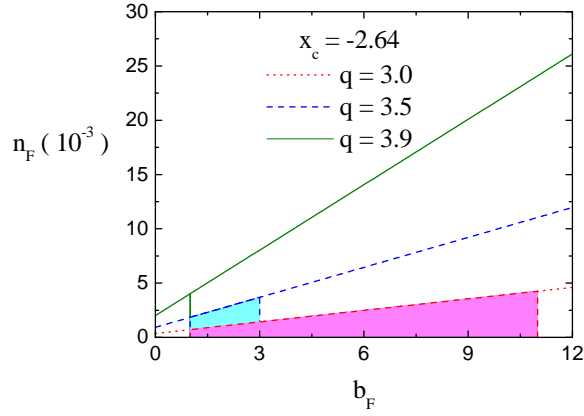


Figure 8: The constraints on n_F and b_F from both the result of Murphy *et al* [21] and that of CMB [22]. n_F values in the graph are scaled by 10^3 . The sloped lines are obtained from QSOs result. The vertical line for each case is obtained from CMB. The shaded regions are allowed ones from both constraints. There is only one b_F -value for $q = 3.9$ (solid line) when we assume that $b \geq 1$. So we can get the upper limit $q < 4$.

From WMAP data, we have obtained a very specific value of $x_c \sim -2.64$ (equally $z_c \sim 13$) for the best fit value. When $x_c = -2.64$ we have obtained the very small $(dw/dz)_{z=0}$, which is consistent with the recent observations. (dw/dz) depends on x_c , which is related to the epoch when the time evolution of ω begins. A smaller value of x_c causes an earlier evolution of ω compared to a larger value of x_c . With a smaller x_c , ρ_ϕ evolves to its present value $\rho_\phi^{(0)}$ at an early epoch and it stays with this value because $\omega \sim -1$. In this case Ω_ϕ is negligible until it reaches its present value and that is similar to when we have the cosmological constant as dark energy. However for some values of x_c the value of Ω_ϕ can be significant at early times. This behavior is quite different from that of a cosmological constant. Thus the difference between the cosmological constant and quintessence is obvious for some values of x_c . Due to CMB consideration we have focused on $x_c = -2.64$ and this has shown the big discrepancy between quintessence and the cosmological constant. We have also found that to be consistent with BBN (*i.e.* $\Omega_\phi^{(BBN)} \leq 0.18$) we need $q \geq 1.50$ when $x_c = -2.64$. Thus this may give one clue for the nature of dark energy. We have made the restriction to the value of q , q_{\min} from the constraint on x_c . As x_c increases, we will get bigger q_{\min} as in Fig. 2. We have also found the upper limit on x_c when we consider the limit of $\Omega_\phi^{(BBN)}$, $x_c \leq -2.60$. We have reached to the lower limit $q \geq 1.50$ when we used $\Omega_\phi^{ls} \sim 0.01$ from WMAP. We have had the similar lower limit on q from the χ^2 -statistic. All of this consideration gives the unique lower limit of $q \geq 1.50$ when we choose $x_c = -2.64$. However there was no upper limit of q from the CMB analysis alone.

We have introduced two more parameters (n_F, b_F) from the generic form of gauge coupling to analyze the evolution of $\Delta\alpha/\alpha$. However we had only three parameters to be fixed after specifying x_c . We have found the viable parameter regions for each parameter by

using $\Delta\alpha/\alpha$ data. From this we have found the well known parameter regions of gauge coupling $(n_F, b_F) \sim (10^{-3}, 1)$ [16]. We have also found the upper limit $q \leq 3.90$ with this analysis.

We have found a viable parametrization of ω with the very specific parameter regions, $x_c = -2.64$ and $1.50 \leq q \leq 3.90$ from the analyses of both the separation of CMB peaks and the time variation of α . We have also found that $-1.00 \leq \omega^{(0)} \leq -0.971_{-0.027}^{+0.017}$ and $1.76_{-0.42}^{+0.29} \times 10^{-4} \leq (d\omega/dz)_{z=0} \leq 0.041_{-0.037}^{+0.016}$ at 95 % CL. Thus we may not see any change of ω at present. Even though the present values of ω and $d\omega/dz$ are almost identical to the values of the cosmological constant, Ω_ϕ evolves from BBN to the present with significant values. Thus this model has the different cosmological behaviors compared to Λ CDM model. We may need to check the similar parametrization and/or more data to investigate the nature of dark energy. We may also need to modify ω to have more than one changeover which can show a non-monotonic behavior.

6 Acknowledgements

This work was supported in part by DOE grant DE-FG02-94ER-40823. We would like to thank Keith.A. Olive for useful discussion.

A Appendix

We have used the analytic approximations for the phase shifts Doran, which we show here. The overall phase shift is given by

$$\bar{\varphi} = (1.466 - 0.466n_s) \left[a_1 r_*^{a_2} + 0.291 \bar{\Omega}_\phi^{ls} \right] \quad (\text{A.1})$$

where the fitting coefficients are

$$\begin{aligned} a_1 &= 0.286 + 0.626\omega_b \\ a_2 &= 0.1786 - 6.308\omega_b + 174.9\omega_b^2 - 1168\omega_b^3 \end{aligned} \quad (\text{A.2})$$

with $\omega_b = \Omega_b^{(0)} h^2$, and $\bar{\Omega}_\phi^{ls}$ is given by

$$\bar{\Omega}_\phi^{ls} = \tau_{ls}^{-1} \int_0^{\tau_{ls}} \Omega_\phi(\tau) d\tau \quad (\text{A.3})$$

and

$$r_* \equiv \rho_r(z_{ls}) / \rho_m(z_{ls}) \quad (\text{A.4})$$

is the ratio of radiation to matter at decoupling. The relative shift of the first acoustic peak is zero, $\delta\varphi_1 = 0$, and the relative shifts of the second peak are given by

$$\delta\varphi_2 = c_0 - c_1 r_* - c_2 r_*^{-c_3} + 0.05(n_s - 1) \quad (\text{A.5})$$

where n_s is scalar spectral index and

$$\begin{aligned} c_0 &= -0.1 + \left(0.213 - 0.123\bar{\Omega}_{l_s}^\phi\right) \times \exp\left(-[52 - 63.6\bar{\Omega}_{l_s}^\phi]\omega_b\right) \\ c_1 &= 0.015 + 0.063 \exp\left(-3500\omega_b^2\right) \\ c_2 &= 6 \times 10^{-6} + 0.137(\omega_b - 0.07)^2 \\ c_3 &= 0.8 + 2.3\bar{\Omega}_{l_s}^\phi + \left(70 - 126\bar{\Omega}_{l_s}^\phi\right)\omega_b \end{aligned} \quad (\text{A.6})$$

References

- [1] A. G. Riess *et al.* [Supernova Search Team Collaboration], *Astron. J.* **116** (1998) 1009 [arXiv:astro-ph/9805201]; S. Perlmutter *et al.* [Supernova Cosmology Project Collaboration], *Astrophys. J.* **517** (1999) 565 [arXiv:astro-ph/9812133]; N. A. Bahcall, J. P. Ostriker, S. Perlmutter and P. J. Steinhardt, *Science* **284** (1999) 1481 [arXiv:astro-ph/9906463].
- [2] B. Ratra, P.J.E. Peebles, *Phys. Rev. D* **37**, 3406 (1988); *Ap. J. Lett* **325**, 117 (1988); C. Wetterich, *Nucl. Phys. B* **302**, 668 (1988); R.R. Caldwell, R. Dave and P.J. Steinhardt, *Phys. Rev. Lett* **80**, 1582 (1998) [astro-ph/9708069].
- [3] P.G. Ferreira and M. Joyce, *Phys. Rev. D* **58**, 023503 (1998) [astro-ph/9711102].
- [4] E.V. Linder and R. Miquel, [astro-ph/0409411].
- [5] T.Barreiro, M.C. Bento, N.M.C. Santos, and A.A. Sen, *Phys. Rev. D* **68** 043515 (2003) [astro-ph/0303298]; W. Hu, *Annals Phys*, **303** (2003) 203 [astro-ph/0210696]; M.C. Bento, O. Bertolami, and A.A. Sen, *Phys. Rev. D* **67** 063003 [astro-ph/0210468]; M. Doran, M. Lilley, J. Schwindt, and C. Wetterich, *Astrophys. J.* **599** (2001) 501 [astro-ph/0012139];.
- [6] N.J. Nunes and J.E. Lidsey, *Phys. Rev. D* **69** 123511 (2004) [astro-ph/0310882]; D. Parkinson, B.A. Bassett, and J.D. Barrow, *Phys. Lett. B* **578**, 235 (2004) [astro-ph/0307227].
- [7] I. Maor, R. Brustein, and P.J. Steinhardt, *Phys. Rev. Lett.* **86**, 6 (2001); Erratum *ibid.* **87** 049901 (2001) [astro-ph/0007297].

- [8] S. Hannestad and E. Mortsell, JCAP, **0409** (2004) 001 [astro-ph/0407259].
- [9] D.N. Spergel *et al.*, Astrophys. J. Suppl **148** (2003) 175 [astro-ph/0302209].
- [10] E. Linder, Phys. Rev. D **70**, 023511 (2004) [astro-ph/0402503]; H.K. Jassal, J.S. Bagla, and T. Padmanabhan, [astro-ph/0404378].
- [11] U. Alam, V. Sahni, T.D. Saini, and A.A. Starobinsky, Mon. Not. Roy. Astron. Soc. **354** (2004) 275 [astro-ph/0311364]; C. Wetterich, Phys. Lett. B **594** (2004) 17 [astro-ph/0403289]; P.S. Corasaniti *et al*, Phys. Rev. D **70**, 083066 (2004) [astro-ph/0406608].
- [12] B. Boisseau, G. Esposito-Farese, D. Polarski, and A.A. Starobinsky; Phys. Rev. Lett **85** 2236 (2000) [gr-qc/0001066].
- [13] R.R. Caldwell; Phys. Lett. B **545** (2002) 23 [astro-ph/9908168].
- [14] A. Lue and G.D. Starkman, Phys. Rev. D **70** 101501 (2004) [astro-ph/0408246].
- [15] V. Sahni and L. Wang, Phys. Rev. D **62** 103517 (2000) [astro-ph/9910097].
- [16] S. Lee, K.A. Olive, and M. Pospelov, Phys. Rev. D **70** 083503 (2004) [astro-ph/0406039].
- [17] W. Hu, N. Sugiyama, and J. Silk, Nature **386** (1997) 37 [astro-ph/9604166].
- [18] W. Hu, M. Fukugita, M. Zaldarriaga, and M. Tegmark, Astrophys. J **549** (2001) 669 [astro-ph/0006436]; M. Doran and M. Lilley, Mon. Not. Roy. Astron. Soc **330** 965 (2002) [astro-ph/0104486].
- [19] A.G. Riess *et al.*, Astrophys. J. **607** (2004) 665 [astro-ph/0402512].
- [20] T. Damour and K. Nordtvedt, Phys. Rev. Lett. **70**, 2217 (1993); Phys. Rev. D. **48**, 3436 (1993); T. Damour and A.M. Polyakov, Nucl. Phys. **B423**, 532 (1994) [hep-th/9401069]; Gen. Relativ. Gravit. **26**, 1171 (1994) [gr-qc/9411069].
- [21] J. K. Webb *et al.*, Phys. Rev. Lett. **87**, 091301 (2001) [arXiv:astro-ph/0012539]; M. T. Murphy, J. K. Webb and V. V. Flambaum, Mon. Not. Roy. Astron. Soc. **345**, 609 (2003) [arXiv:astro-ph/0306483].
- [22] G. Rocha, R. Trotta, C. J. A. Martins, A. Melchiorri, P. P. Avelino and P. T. P. Viana, New Astron. Rev. **47**, 863 (2003) [arXiv:astro-ph/0309205].